

An Optomechanical Coin Flip: Wavelength-Modulated, Erbium-Powered Rotations in a Levitated System

George Winstone,^{1,2} Maddox Wroblewski,^{1,3} Lars Forberger,⁴ Zhiyuan Wang,¹ Shelby Klomp,¹ Scott Grudichak,¹ Shafaq Gulzar Elahi,¹ Yuqi Qian,^{1,2} Miriam M Flórez,⁵ Zhaojie Feng,⁴ Peter J. Pauzauskie,^{4,6} and Andrew A. Geraci^{1,2}

¹*Center for Fundamental Physics, Department of Physics and Astronomy, Northwestern University, Evanston, Illinois 60208, USA*

²*Center for Interdisciplinary Exploration and Research in Astrophysics, Department of Physics and Astronomy, Northwestern University, Evanston, Illinois 60208, USA*

³*Department of Physics, The University of Texas at Austin, Austin, TX 78712, USA*

⁴*Department of Materials Science & Engineering, University of Washington, Seattle, Washington 98195, USA*

⁵*IQQI, Innsbruck, Austria, EU*

⁶*Physical and Computational Sciences Directorate, Pacific Northwest National Laboratory, Richland, Washington 99352, USA*

(Dated: February 25, 2026)

Optical levitation of nano-scale systems offers a pathway to highly sensitive rotation measurements, which are critical for advancing gyroscopic technologies. While prior studies have primarily focused on controlling rotational degrees of freedom of optically levitated particles via modulation of optical power, polarization, and ambient pressure, here we demonstrate wavelength-controlled rotation of the “coin-flip” mode in optically levitated NaYF hexagonal prisms doped with erbium by modulating the wavelength of a secondary pump beam. By switching the pump light wavelength, we precisely modulate the particle’s rotation rate in a binary fashion, encoding the ASCII message “hello” in its rotational frequency. Finally, we observe long-term bimodal periodic dynamics in the rotational motion of a levitated prism that are suggestive of a Dzhanibekov (or tennis-racket)-like effect.

I. INTRODUCTION

Rotational effects in levitated optomechanics have grown into a topic of significant interest to the scientific community over recent years [1] for a variety of reasons including gyroscopic navigation, biological analysis [2], observing the Casimir torque [3, 4], pressure sensing, and the possibility to extend the boundaries of fundamental physics by observing decoherence-resilient quantum dynamics of a macroscopic system [5]. Indeed, the fastest-spinning man-made objects are optically levitated nanoparticles [6, 7].

Additionally, significant scientific effort has been expended in recent years on the production of massive quantum superposition states. Wave-like behavior and matter-wave interference has been experimentally demonstrated for electrons [8], neutrons [9–11], atoms [12–16], and even complex molecules and clusters [17–19], and levitated optomechanical systems represent a promising platform to achieve delocalized quantum states and wave-like behavior in systems with several orders of magnitude larger mass [20–23]. Levitated nanoparticles have been able to be cooled to the quantum ground state of their trapping potential for their translational degrees of freedom [24–27], librational degrees of freedom [28], and recent work has shown a quantum wave packet delocalization beyond the size scale of a nanoparticle [29]. Decoherence effects represent one of the greatest challenges in achieving macroscopic spatial superpositions with large masses [30]. A number of methods to deal with

decoherence effects in massive macroscopic state generation have been proposed. These include performing the interference quickly [31], or performing the interference at a very low temperature to suppress decoherence effects [30].

In this context, degrees of freedom that are resistant to decoherence effects are especially valuable. In particular, quantum mechanical equivalents of free rotations are expected to display strong resilience to classical noise channels [5]. These advantages have also been projected to be observed for the quantum tennis-racket-effect [32]. Notably, the appearance of quantum dynamics in the tennis-racket-effect is independent of the rotor mass [32], potentially allowing for the creation of larger quantum superpositions than when created via linear translational states. Recent experimental work in cooling the librational degrees of freedom of an optically levitated particle [33] specifically targets the quantum tennis-racket-effect as a goal, making this exploration of such a topic in an optically levitated system a timely endeavor for the community.

In the macroscopic world, torsion balances are some of the most sensitive experiments constructed on a tabletop and provide some of the best limits in setting bounds on existing physical laws and exploring new novel physics [34, 35]. In the world of nano- and micro-scale levitated optomechanics, the same fundamental principle is possible at orders of magnitude lower length scale, with the librational bounds of an optically levitated microparticle providing the arms of the torsion balance [36].

Gyroscopes, particularly optically levitated nanoparticle-based gyroscopes, have garnered significant attention in recent research [1] with the potential for parts-per-billion (ppb) scale factor stability gyroscopes via optical levitation of nanospheres and microspheres. One of the requirements is a high moment of inertia, low-noise levitator with center-of-mass cooling that can be rotated extremely quickly in free space while decoupled from its environment [1]. Optically levitated nanoparticles also show very low damping rates when spun around the most symmetric axis [37]. Together, these factors of high rotational speeds, low damping, and the potential to feedback cool the non-rotating degrees of freedom to ground state (thus reducing the rotor noise from the gyroscope perspective) suggest a potentially rich platform for gyroscope development. Our experimental work in this paper adds another method into the toolbox for controlling the rotational states of optically levitated systems.

Finally, to place our work into additional context, significant effort has recently gone into engineering ‘smart particles,’ which are built or grown in bespoke topologies and shapes, and in some cases have additional interesting and useful internal degrees of freedom added via doping. One such example is β -NaYF hexagonal prisms which have been optically levitated [38, 39] and can be doped with lanthanides such as erbium or ytterbium to allow for solid state cooling [40, 41]. Similar flat geometries, which may prove to be advantageous for overcoming photon recoil heating [39], might also be amenable to printing top-down degrees of freedom with classic photolithography techniques, potentially allowing for a convergence of top-down and bottom-up added degrees of freedom in a levitated system.

In this work, we introduce control of the rotational frequency of a 5% Er: β -NaYF levitated system by tuning the wavelength of a pump laser. This is enabled through use of the erbium dopant as an atomic engine to facilitate the driving/control. Rotational frequency control like this has only previously been achieved through tuning of optical power and/or polarization (utilizing the objects shape [42], or birefringence [43], or structured light with orbital angular momentum [44]).

Using wavelength as an additional control parameter offers potential advantages over intensity and/or polarization tuning. Wavelength modulation can in principle adjust the rotational frequency without altering the total optical power at the trap, thereby avoiding unwanted changes to translational confinement. Wavelength based control also does not have the requirement of using a birefringent material or appropriate geometry amenable to polarization based control.

II. EXPERIMENTAL SETUP

A conceptual schematic overview of the experiment is given in Figure 1, along with the major results, while the

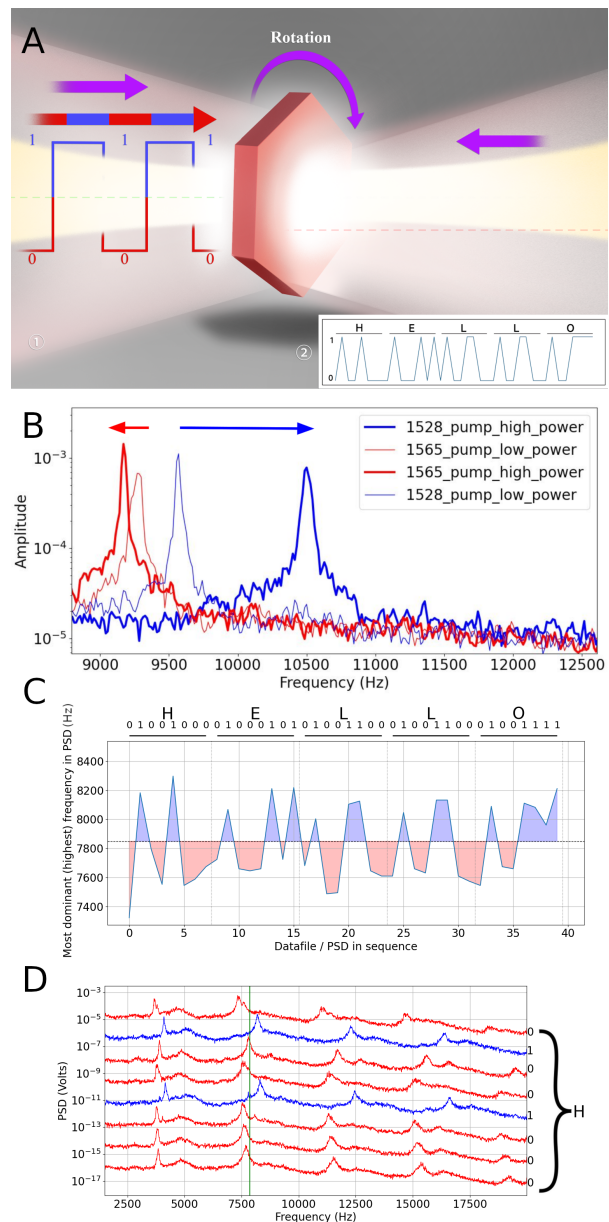


FIG. 1. **A:** Conceptual figure of an optically levitated hexagon receiving a bitwise binary control signal in the form of red- and blue-detuned (with respect to the trapping light) pumping laser, which causes the hexagon to rotate faster or slower depending on the wavelength of the control signal. Blue causes the hexagon to rotate faster while red either causes less change or causes it to slow down depending on the background pressure of the system. **B:** The frequency domain data of the free rotational motion of an optically levitated hexagon when being pumped with red-detuned and blue-detuned light at 2 mbar pressure. This data is zoomed in to the region of interest of the highest amplitude peak in the Fourier spectrum of the optically levitated test mass’s motion. Here low power indicates 0.1 mW of pump power and high indicates 31 mW of pump power. **C:** Hello world sequence generated by changing the wavelength of the applied pump beam (blue pump = 1, red pump = 0). Encoded ASCII sequence is sufficiently resilient to long term drifts to encode a 40-bit message in wavelength space, which is then read out in the mechanical motion of the particle. **D:** Waterfall plot of a single ASCII character from the ‘hello’ sequence (‘H’) in its constituent bits. Note that the levitated hexagon used in **B** is a different one than that used for **C** and **D**.

detailed experimental setup is given in Figure 2. The trap is formed by counterpropagating 1560 nm trapping light with a 12.5 μm focus. We optically trap 5% doped 5 μm diameter, 200 nm thick NaYF hexagons as shown in the SEM Appendix Figure 11. The pump light is provided by a separate laser (a pure photonics PPCL), which is fiber-coupled into the trapping region via a Thorlabs 2 \times 2 PM 90:10 splitter - since it is very close to the wavelength of the primary trapping laser. A wavelength division multiplexer (WDM) is used to counterbalance the insertion loss on the other side of the trapping region - but is not actively used in the experiment - for visual clarity the WDM is omitted from the experimental diagram. In contrast to the counterpropagating trapping light, the pump light only enters the trapping region from one side of the optical trap - this is specifically to avoid the creation of a second competing optical lattice. In particular, pump light entering the trapping region from one side generates the potential systematic error of lowering the center of mass frequencies with increased optical power of the atomic resonance (since it pushes the test mass further away from the optimal/highest frequency trapping region), whereas a second competing lattice might raise or lower the center of mass frequencies depending on the alignment of the first and second lattice. Given the lattice overlap depends on wavelength, this could represent an unacceptable source of systematic error.

The optical detection scheme for the levitated test masses is broadly explained in Ref.[38], with a few small changes having been made between [38] and this work. In particular, the setup described in Ref. [38] contains a detection channel called 'fiber-line', and in this work we also create an additional similar detection channel, in which a moveable free space detector is placed after the fiber output coupler of the experiment for an additional degree of tunability. All of the data in this work is taken with this new detection scheme.

III. EXPERIMENTAL RESULTS

A. Shifting the central rotational frequency by changing the color of the applied pump light

The free body rotational dynamics of optically levitated Rayleigh scale objects have been well studied in the past [45]. Furthermore, control over the rotational degrees of freedom has been shown previously by modulating the optical trapping power and pressure of the system [46–48]. Here, for the first time, we show control over the rotational degrees of freedom by modulating the wavelength of the incoming laser light. Since the NaYF hexagons are doped with erbium ions (5% by mass), the strongly wavelength dependent absorption spectrum of the erbium ion increases the net extinction cross section of the levitated object substantially at a certain wavelength, this enables this level of control over the free body dynamics with a relatively small amount of wavelength

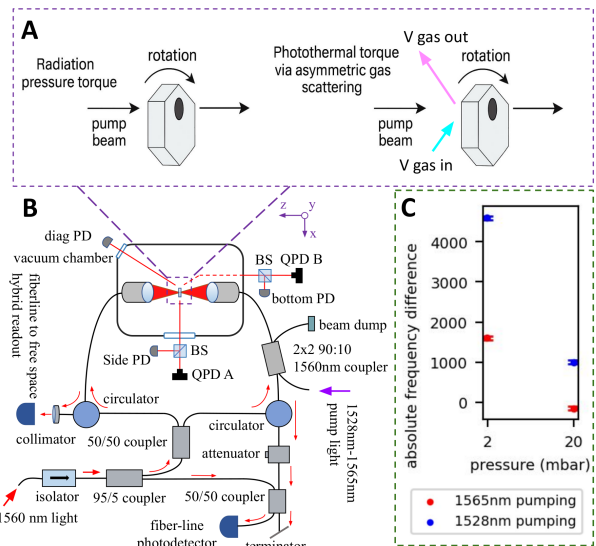


FIG. 2. **A:** Angular momentum injection mechanisms. (left) In the first mechanism the momentum of injected blue-detuned photons is turned directly into rotational angular momentum by the photons being absorbed by the erbium ions embedded in the NaYF crystal matrix - the photons literally push the optically levitated hexagon to spin faster. (right) In the second mechanism, the blue-detuned photons are turned into rotational angular momentum by being absorbed by the erbium ions embedded in the NaYF crystal matrix as heat. The hotter surface temperature of the levitated hexagon then pushes incident background gas particles away faster than they impacted (the hot surface rocket effect), thus leading to a faster total free body spin rate. **B:** Experimental setup: 0.5 W of 1560 nm counterpropagating trapping light (provided by NKT C15 laser) is split in fiber and fed to the trapping site at a beam waist of 12.5 μm , red detuned (1565 nm) and blue detuned (1528 nm) light (provided by a separate Pure Photonics PPCL laser) is fed to the trapping site along one arm of the counterpropagating fibers and thus trapping light. The power of the pump beam incident on the levitated hexagon can be varied across a range of 0.1 mW to 50 mW. **C:** The effect of the detuned photons on the spin rate as a function of pressure is explored experimentally over one order of magnitude, for two different wavelengths. For each pressure and wavelength, the frequency difference from 31 mW to 0.1 mW of pump power is shown.

modulation. By controlling the wavelength of the pump laser, we can change the center of mass rotation frequency of the levitated hexagon.

The damping experienced by the free body rotational motion of the hexagon is determined by the mostly constant background gas pressure inside the chamber. Increasing the torque being injected into the system increases the speed at which the hexagon rotates, while decreasing it reduces the speed at which it rotates. We propose two mechanisms by which the pump light may be transformed into torque (see Figure 2A). In the first, blue detuned photons are directly transformed into angular momentum through being absorbed at a higher efficiency by the erbium dopants that are on resonance with

the wavelength of the light, if the center of the pump beam is slightly off axis with the center of the levitated hexagon.

In the second mechanism blue detuned photons are indirectly transformed into torque by being absorbed at a higher efficiency by the erbium dopants and transformed into heat, this changes the internal temperature of the levitated NaYF prism: A gas molecule incident on a hot surface rebounds with a higher velocity characteristic of the higher surface temperature. Since momentum is conserved this leads to a thrust on the surface. This is often referred to as the Crookes radiometer effect [49]. Naturally, this requires an inhomogeneous distribution of temperature over the levitated hexagon - a slightly asymmetric optical trap or distribution of dopants would be sufficient. Such localised heating effects causing localised surface thrust have been observed in levitated microparticles before [50][51].

The pressure dependence of the rotation rate is shown in Figure 2C over an order of magnitude in pressure. The difference in rotation rate between red and blue detuning is a function of pressure, indicating that gas collisions play a significant role in the observed dynamics.

To roughly estimate the torque involved in sustaining such a rotation process, we approximate the hexagonal prism as a cylindrical disc of radius $r = 1.5 \mu\text{m}$, and thickness $t = 0.2 \mu\text{m}$. Given the moment inertia for the “coin-flip” mode of $I = \frac{1}{4}\pi\rho r^4 t$, an angular acceleration α applied to the system in the presence of the viscous drag from the surrounding gas with a rotational damping rate of $\Gamma_{rot} = P\pi r^4 / (Iv_{gas}\sqrt{2\pi})[1 + \frac{\pi}{4} + \frac{t}{r} + \frac{t^2}{2r^2} + \frac{t^3}{4r^3}(1 + \frac{\pi}{6})]$ [52] would result in a steady state rotational velocity $\dot{\theta}_z = \alpha / \Gamma_{rot}$. Here P is the background gas pressure and $v_{gas} \equiv \sqrt{k_B T / m_{gas}}$ is the characteristic thermal velocity of gas molecules of mass m_{gas} at temperature T . To sustain a rotation speed of $\dot{\theta}_z \approx 4 \text{ kHz}$, corresponding to the strongest observed rotational signal in the photodetector at twice this frequency $2\dot{\theta}_z \approx 8 \text{ kHz}$, the needed torque is a approximately 9 aN·m. Such a torque could be imparted for example if the two optical beams are offset by a small amount δ . Assuming an effective extinction power P_{ext} that could be a combination of scattering and absorption, the angular acceleration applied to the system in this case is approximately $\alpha \approx P_{ext}\delta / (cI)$ where c is the speed of light. We find that an offset of $\delta = 1 \mu\text{m}$ and $P_{ext} = 30 \text{ mW}$ would be sufficient to provide the required torque, or an equivalent torque from radiometric forces would produce similar behavior. A more detailed estimate of such radiometric torques would require modeling the distribution of dopants, estimating the internal heating, and modeling the gas flow dynamics and is reserved for future work.

Here we have neglected the restoring force of the trap which would oppose free rotation of the hexagon for sufficiently small applied torques if the hexagon were starting trapped in its upright configuration as in Ref. [38]. We expect these forces to be strongly acting only when the tilt θ_z of the hexagon is smaller than $\sim \lambda/8r$. For an

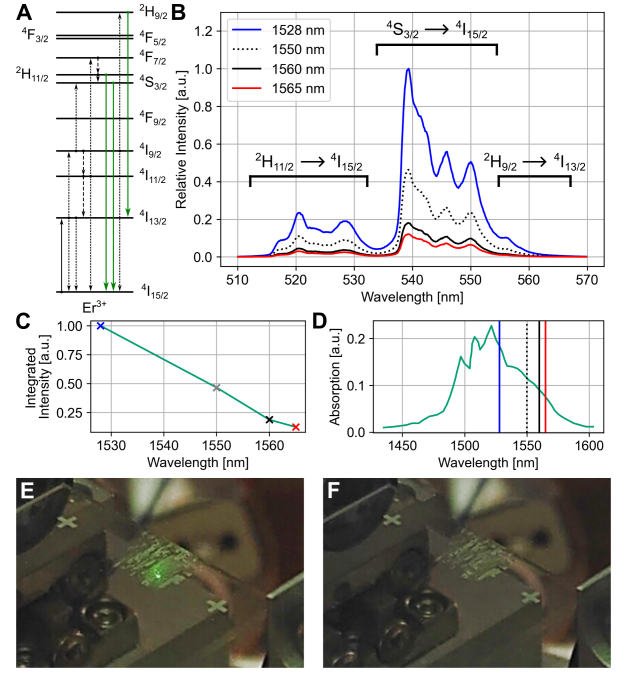


FIG. 3. **A:** Erbium energy diagram and green emissions. **B:** Green erbium photoluminescence measured at different pump wavelengths. **C** Integrated intensity of the green erbium emission plotted against the pump wavelength. **D** Digitized and replotted literature absorption spectrum of 5% erbium doped β -NaYF [53]. **E:** Optically levitated in free space just below the slide, 5% erbium doped β -NaYF illuminated with 1560 nm trap light emitting green light with sufficient intensity to image with a long exposure ($\sim 60 \text{ s}$). **F:** Undoped optically levitated β -NaYF suspended in free space immediately below the launch slide. Contrast and brightness of the images is digitally enhanced.

axial trapping frequency of 5 kHz, We roughly estimate that external torques above a threshold value $\tau_{crit} \approx 2.5 \text{ aN}\cdot\text{m}$ would be sufficient to initiate the coin-flip rotation.

An image of strong green emission from upconverted photons is given in Figure 3 for a trapped particle. A simplified energy level diagram of the erbium dopants and pump wavelength-dependent photoluminescence is given in Figure 3 and the proposed multi photon relaxation pathway leading to green light emission is highlighted. The intensity of emissions in the top right inset follows absorption measurements from the literature [53] and illustrates the efficiencies at detuned wavelengths. As further explained in the Appendix the rotational motion visible in this experiment displays a significantly higher detection efficiency / signal to noise ratio (SNR) than the translational degrees of freedom. We attribute this to the larger amount of material being moved through a larger space in a free rotation compared to a translation. A free rotation of a high aspect ratio object with a diameter of microns moves its whole mass a full 2π steradians about its own axis. This is several orders of magnitude more matter moved through space than an objects translating

some 10's of nanometers (thereby perturbing the incident light beam more).¹

B. Binary encoding of a 40 bit message onto the rotational degree of freedom via wavelength modulation - "Hello world"

Rotational degrees of freedom are extremely sensitive to their boundary conditions and environment, variables such as; pressure, laser power, laser relative intensity noise (RIN), etc. Long term studies of rotating levitated micro and nanoparticles often observe significant variations in the rotational frequency over time - especially under non UHV conditions. Rotating particles are sometimes locked to an external reference to address this, leading to ultra stable mechanical rotors [55].

To demonstrate our degree of substantial control over the system, over the level of the natural systematic errors of the instrument response and experiment noise, we chose to encode a binary message into the wavelength pump into the system, and then we read that message out in the center of mass rotational frequency of the levitated hexagon.

A traditional first case message to encode is often 'hello world'. In this case, we chose to just encode the word 'hello'. The message was encoded into a binary sequence by changing the wavelength of the applied pump beam. Blue detuned (with respect to the trapping beam) pump light (1528 nm) represents a bit of 1, Red detuned pump light (1565 nm) represents a bit of 0. The non pump light (1560 nm) runs at an optical trapping power of 500 mW in a counterpropagating configuration (Figure 2). The encoded ASCII sequence is sufficiently resilient to long term/systematic drifts in the rotational frequency to encode a 40-bit message in wavelength space, which is then read out in the mechanical motion of the particle as the frequency of the rotational peak. This is shown in Figure 1. Throughout the experiment either 0.15 mW (low-power case) or 31 mW (high-power case) of pump laser power reaches the levitated hexagon. The power dependence is explored briefly in Figure 1B and Figure 2C. At high pressure red-detuned pumping slightly reduces the spin speed of the hexagon with increasing power, while blue-detuned pumping increases the spin speed. At lower pressure increasing the pump power at both red- and blue-detuned pumping increases the spin speed.

C. Long term scans - tennis racket effect

Since angular momentum is constantly being injected by the pump light into the rotating hexagon, it does not immediately spin down, and can rotate for days or weeks on end. This allows us to observe long term rotational dynamics of the optically levitated test mass. Note that in our experimental setup, hexagons that are not doped with erbium tend to slow down their rotation on the time scale of tens of minutes to hours - (Figure 8), and then eventually stop rotating entirely. We attribute this to lack of a constant driving force keeping the rotation going.

The Dzhanibekov effect, or tennis racket effect, describes how objects with three distinct axes of inertia behave during free rotation. While they rotate stably around their longest and shortest axes, rotation around the intermediate axis is unstable, causing the object to flip about this axis, exhibiting metastable rotations in each orientation. We observe slow transfers in rotational frequencies (and thus angular momentum) of the levitated hexagon interspersed with rapid flips. These slow transfer invert signs (direction) at periodic points in the long term data set. We interpret these long-term periodic flips to be similar physics to that of the tennis racket effect (Dzhanibekov effect), in which a rotating object with the right mass distribution periodically flips about its prime axis of rotation [56]. A popular and intuitive demonstration of this effect is spinning a spanner(wrench) in zero gravity on the international space station. This effect can occur for both a classical and quantum mechanical rotor [32].

Several features indicative of tennis racket like effects - strictly in the classical regime - are delineated in long term frequency space traces of a rapidly rotating optically levitated mass composed of NaYF hexagons. Two effects indicative of tennis-racket-like effects are shown in the dataset: 1) Slow drifts in the rotational frequencies leading up to 2) flipping/inversion points, figure 4. Qualitatively this is the same dynamic behaviour as the flipping spanner/wrench freely floating on the ISS [57].

Finite element modeling to derive the exact flipping period of the hexagon from the set of physical inputs given in the work will be a topic of near term future numerical studies, and is beyond the scope of this experimental work.

However, it should be noted there are several pieces of physics that are not included in the simple naive tennis racket model, such as a net flow of energy into the system driving the rotational motion, significant damping, significant center of mass motion in non rotational degrees of freedom and the existence of non trivial couplings to additional degrees of freedom in the system. All of these are present in our experiment and are non-trivial to model.

¹ Recent work has computed the information radiation patterns (IRPs) for bound librational states of motion through Fisher information approaches [54], however unbound free rotations were not considered in that work.

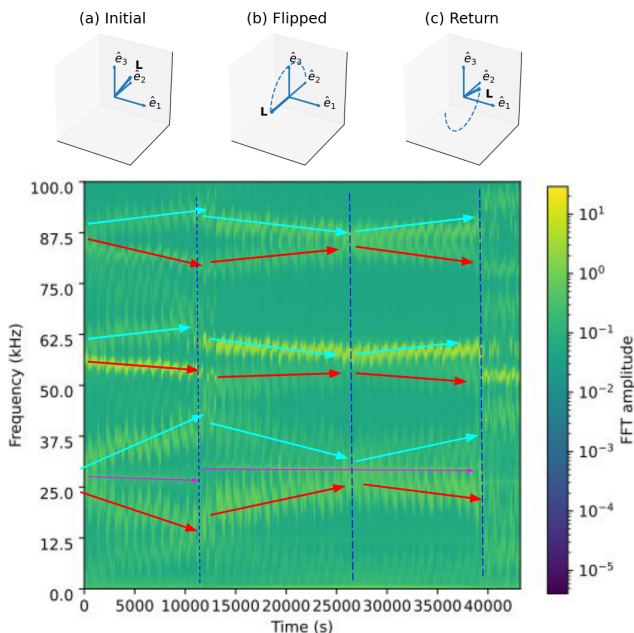


FIG. 4. Tennis racket effect like flips delineated in a long term dataset for a levitated mass. A conceptual example of a possible orientation of the hexagon during the experiment is presented.

D. Green light generation - NIR to visible upconversion

When optically trapped, the erbium-doped β -NaYF emits green light upconverted from the 1560 nm trapping laser. This single particle emission is bright enough to be imaged with a regular camera and a long exposure time (about 60 s) as shown in Figure 3. The photoluminescence (PL) is caused by an overlap of the trapping wavelength with the $^4I_{15/2} \rightarrow ^4I_{13/2}$ electronic transition, resulting in absorption. Consecutive excited-state absorption (ESA), energy transfer (ET) between erbium dopants, and non-radiative relaxation will lead to a population of the $^2H_{11/2}$ and $^4S_{3/2}$ energy levels, which emit green photons when radiatively relaxing to the $^4I_{15/2}$ ground state as schematically illustrated in Figure 3. Furthermore, the emission from the $^2H_{9/2}$ to the $^4I_{13/2}$ excited state falls into the green wavelength range as well [58]. The independently obtained spectroscopic data in Figure 3 show emissions from transitions to the electronic ground state of erbium, but no contributions from excited state absorption. While the irradiance was much lower than in the trapping setup, this absence is promising for complication-free ratiometric thermometry [59]. The relative and integrated intensity of the green photoluminescence illustrates the influence of the pump wavelength with a decrease from blue-detuned to red-detuned excitation, showing the same trend as literature absorption measurements of 5% Er: β -NaYF [53]. It should be noted that while the emission appears green to the eye, there are many more emission lines due to the rich electronic

structure of Er^{3+} . Spectra from 500 nm to 1000 nm are presented in Appendix Figure 10.

The observation of strong emission points towards two potential use cases in future work. First, the upconverted light could be used for virtually background-free detection of the particle dynamics in the trap. Second, in situ contactless thermometry is possible given that the ratio of emission from the $^2H_{11/2}$ and $^4S_{3/2}$ excited states is known to be very sensitive to changes in temperatures.

IV. CONCLUSION

In summary, we demonstrate the first wavelength-detuning-based driven rotational control of a high aspect ratio levitated β -NaYF microhexagon doped with erbium. This represents the first foray into *wavelength* based rotational control in an optically levitated system.

The ability to tune the free rotational frequency via wavelength modulation suggests a pathway to improved rotational stability and therefore sensitivity that does not depend exclusively on modulating power or polarization at the trap (as has been done previously in the literature). To achieve high levels of gyroscopic performance, systems based on micron scale optically levitated test masses require high degrees of feedback control [1], being able to tune several variables independently that are not highly coupled to each other is a valuable element to have for the operation of any closed loop system.

Finally, other optically levitated morphologies (such as spheres, dumbbells and nanorods) have been developed to routinely enable a high degree of control of rotational degrees of freedom. In developing control systems for high aspect ratio particles we note a few general use cases for the rotational degree of freedom for these particles: (i) The rapidly rotating optically levitated hexagons produce an optomechanical frequency comb of up to the 20th harmonic - opening up potential applications for broadband sensing with mechanical frequency combs; (ii) Given the quantity of light emitted in the green by upconversion, there exists significant potential for background and trapping light free detection by counting emitted green photons; (iii) due to their extremely high aspect ratio of optically levitated disk likes [38], they should make excellent pressure sensors while rotating - with a high mass to area ratio in the parachute-like axis and an extremely low ratio in the anti-parachute axis - potentially allowing for shape dependent calibration within the same sample. Furthermore the fine control over temperature and spin rate may present applications for any rotation based optofluidic propulsion, mixing, or sensing[60]. These general use cases aside, a potentially highly impactful application of our work here is likely gyroscope development, inertial sensing, and navigation. With this work we have expanded the toolbox of possible mechanisms to control rotation in optically levitated spinning mass gyroscopes.

Lastly and finally we observe long-term rotational dy-

namics qualitatively consistent with tennis-racket-like behavior in an optically levitated system - also for the first time to the best of the authors knowledge. This is expected to have potentially significant applications in high mass matter wave interferometry due to the potential natural resistance of these modes to decoherence [32].

V. APPENDIX

A. Comparison: spinning and non tennis racketing, spinning and tennis racketing, and non spinning hexagons.

In figure 5 data is presented for optically levitated hexagons under several distinct states. A: a spinning and non tennis racketing levitated hexagon undergoing free rotations, B: a spinning and tennis racketing levitated hexagon undergoing free rotations and experiencing the directional flips consistent with a tennis racket like effect. C: a non spinning levitated hexagon translating in bound vibrations/librations in the standing wave potential defined by the counter propagating beams. The vertical interruptions in C are due to intermittent failures in the data system over long time scales and do not represent particle loss. Experimental conditions were a trapping power of 500mw and a roughing pump pressure of 2mbar.

1. Effect of the vacuum pump on the rotational frequency

Since for a rotating system the free body rotating frequency is directly dependent on the systems pressure, the pressure set point of the vacuum pumping system and subsequent oscillatory behavior around said setpoint manifests as a distinct oscillation of the free-body rotational frequency in the long term datasets of rotating hexagons, this frequency is significantly higher than the other identified dynamics within the system. Note the approx 15 minute oscillations in figure 5 subplots A and B.

B. Auxiliary data - full recorded frequency spectrum of the FFT for the red/blue pumping experiment.

For completeness, Figure 6 shows the full frequency spectrum of the data given initially in Figure 1, showing all the higher order harmonics of the freely rotating mode up to the ~ 20 th order. Of note is that the rotational mode detection efficiency completely overpowers that of the translational mode detection efficiency. When a high-aspect-ratio levitated hexagon starts spinning, e.g. in its “coin-flip” mode, its translational dynamics tend to be difficult to observe in the motional power spectrum.

We primarily attribute this difference in detection efficiencies to the amount of material that moves through space - associated with a particular degree of freedom. A large change in the intensity of light striking the photodetector occurs as the light reflecting from the face of the hexagon sweeps out a very large set of angles as the particle rotates.

For means of comparison, the translational thermal motion (assuming it is simple harmonic oscillator in con-

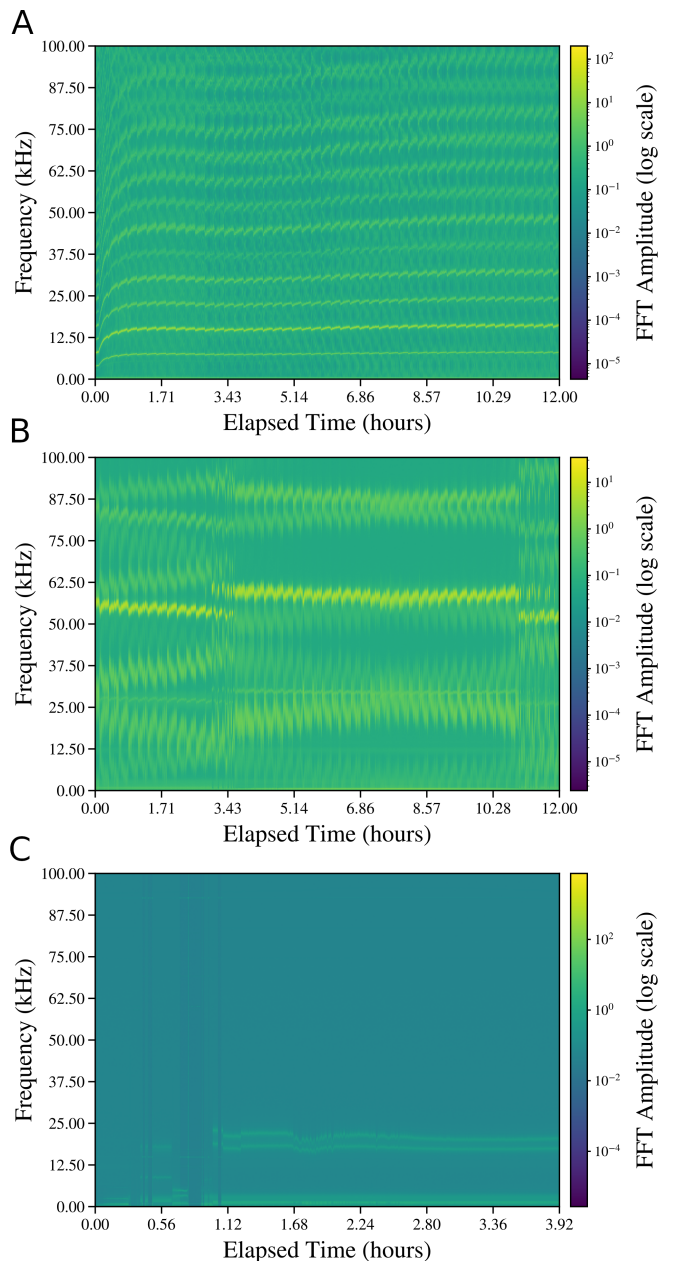


FIG. 5. Comparison: A: spinning and non tennis racketing levitated hexagon, B: spinning and tennis racketing levitated hexagon, C: non spinning levitated hexagon translating in bound vibrations/librations in the standing wave. The vertical interruptions in C are due to intermittent failures in the data system over long time scales and do not represent particle loss.

tact with a thermal bath at ~ 300 K) for a $5 \mu\text{m}$ diameter 200 nm thick levitated hexagon is on the order of magnitude of tens of nanometers [38]. By contrast the freely unbound rotating motion of a disc moves its entire mass about its own axis, at a radius diameter of $5 \mu\text{m}$.

In the case of another commonly studied rotating optically levitated object - the nanodumbbell [45] the amount of material moving through space is about equal for the

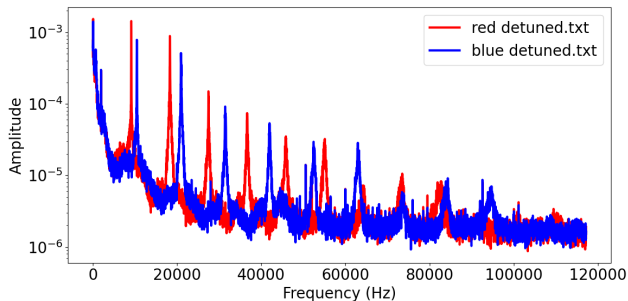


FIG. 6. Full frequency spectrum of the rotating hexagon shown initially in Figure 1, the figure depicts the red and blue detuning of the free rotational motion of an optically levitated hexagon when being hit with red and blue detuned light. The applied pump power is 31 mW in both cases.

rotational degrees of freedom - the radius of the dumbbell is of order ~ 100 nm, with thermal motion on the hundreds of nanometers scale. We attribute this difference of characteristic scales (the translational and freely rotating modes of small low aspect ratio objects and larger high aspect ratio objects) as the reason for why the x, y, z modes disappear almost completely in the detectable output for the optically levitated hexagon while all modes remain visible in the case of rapidly spinning optically levitated dumbbells [45].

The scattered information patterns for a rotating / librating optically levitated test mass is a topic for future investigation, building on existing methods [54].

C. Effect of blue and red light detuning on the optomechanical damping

For the model of the linear translational degrees of freedom of an optically levitated harmonic oscillator, the damping tends to be dominated by collisions with background gas molecules.

The dependence of this damping upon the temperature of the background gas is an extremely complex function of the temperature itself, pressure, gas species, and the geometry of the object. However in the specific limit explored in this paper, we find that the damping tends to increase as we increase the amount of applied blue detuned pump light - which is likely increasing the internal temperature of the levitated hexagon.

The dataset shown in Figure 7 consists of 40 measurement files that already had Fourier transforms applied and was processed on the Northwestern Quest Supercomputing Cluster using the Quest-Analytics Jupyter-Hub environment. Signal processing was performed using the SciPy library (specifically `scipy.ndimage` and `scipy.signal`), along with NumPy for numerical manipulation and Matplotlib for visualization. Peak analysis in particular made use of functions from `scipy.ndimage` and `scipy.signal`.

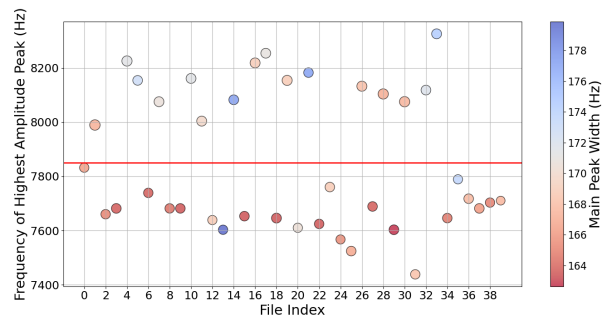


FIG. 7. The same 'Hello World' dataset as in figure 1 is analyzed to investigate correlation between increased internal temperature of the levitated hexagon from being irradiated with blue detuned light and higher optomechanical damping. The frequency of the highest-amplitude spectral peak for each measurement file under blue and red detuned pumping conditions is plotted against the file index in the same order as in figure 1. As in figure 1 - blue detuned datapoints have a higher frequency, while red detuned datapoints have a lower frequency - leading to the bimodal distribution in frequency space. Marker size is proportional to the peak height (amplitude). The colour of the points on a blue-red scale denotes the width of the measured peaks - corresponding to the optomechanical damping. On average, the peaks on the top half of the bimodal distribution - higher frequencies - blue detuned - tend to be wider in frequency space, this is consistent with increased damping due to internal heating of the levitated particle. (for peak detection and peakfinding, some smoothing of the dataset is required in frequency space, in this case we pick $\sigma = 64$, representing the standard deviation of the Gaussian distribution convolved with the measurement signal)

The voltage signal was first smoothed to reduce high-frequency noise using a one-dimensional Gaussian filter:

$$V_{\text{smooth}}(t) = \text{gaussian_filter1d}(V(t), \sigma).$$

Several values of the Gaussian width parameter σ were tested in order to identify an optimal balance between noise suppression and preservation of peak structure.

Peak detection was then carried out using `scipy.signal.find_peaks`. To determine a consistent threshold for peak prominence across all signals, a data-driven prominence threshold was defined as

$$P_{\text{threshold}} = [\text{percentile}(V_{\text{smooth}}, 95) - \text{percentile}(V_{\text{smooth}}, 5)] \times 0.1$$

This percentile-based scaling ensured that peak selection was robust to variations in overall signal amplitude. Peaks exceeding this prominence threshold were retained, and their widths were subsequently extracted using the `peak_widths` function for additional quantitative characterization [61–63].

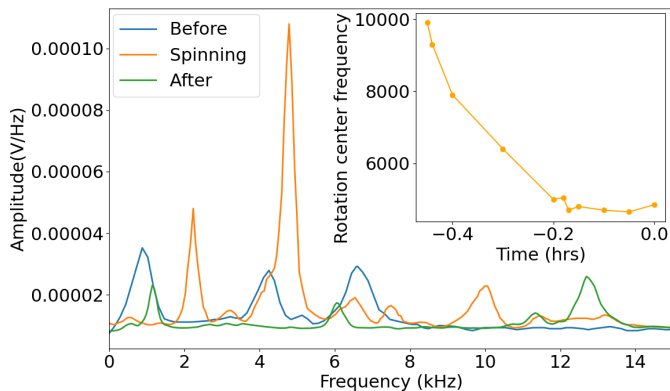


FIG. 8. Main figure: In this dataset an undoped optically levitated NaYF hexagon is initially observed to be levitated normally, with all librational degrees of freedom bound within the potential of the standing wave and the flat face of the hexagon is aligned to the standing wave propagation axis. The hexagon is then perturbed by a random background fluctuation and begins to rotate freely about its axis, first slowing down to a lower rotational free body rate and then eventually returning to bound motion standing up within the standing wave optical potential. The transition spinning motion is accompanied by an increase in the signal to noise ratio / Q factor of the most dominant peak of almost an order of magnitude. The significance of this dataset is that 'single' well-formed hexagons can exhibit high speed rotation - 'dumbbell' like configurations are not required, although dumbbells (accumulations of two or more hexagons into bimodal mass distribution) may also be levitated and rotating within the trap in other runs. NaYF hexagons without erbium dopant tend to spin down in a matter of hours. Inset: The freely rotating motion of the optically levitated hexagon rings down without active injection of angular momentum via optical pumping of atomic dopants into momentum to maintain the rotation. The pressure is kept constant at 2 mbar throughout the experiment.

D. Rotational dynamics - further observations

1. *Single hexagons can be trapped 'normally', start spinning, and then return to being normally trapped.*

Figure 8 shows the **same** hexagon before starting a spin cycle, while rotating, and after spinning down into a well behaved bound position. This demonstrates that 'single' hexagons can display free body unbound rotations and that a dumbbell like shaped cluster is not required. This is a different hexagon than those used for the other results of this work, however it is trapped in the same setup under similar experimental conditions of power and pressure. The 'ringdown' of this hexagon during the spinning state is given in the inset of Figure 8.

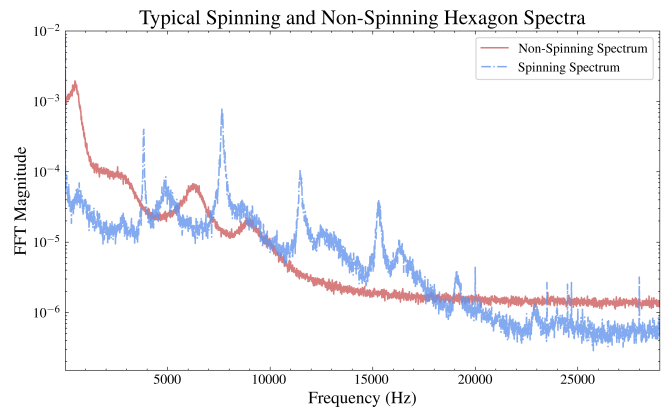


FIG. 9. Comparison of hexagons bound to the optical lattice translating over small amplitudes and freely rotating hexagon PSDs overlaid.

2. Rotating and non rotating trapped hexagons comparative PSDs

Figure 9 shows two different hexagons, one bound in stable translations and librations, and one undergoing free rotations about its axis - taken under similar experimental conditions. The PSDs of freely rotating high aspect ratio hexagons tend to have one dominant frequency with many harmonics - the translational frequencies are almost entirely suppressed out of the PSD. Non freely rotating hexagons display the usual \leq degrees of freedom. It should be noted however that identification of an optically levitated objects shape and dynamics from a single PSD is extremely difficult since the parameter space is so degenerate. The greatest point of identification for rotational dynamics is the rotational frequency dependence on pressure.

3. Rotating hexagons with no Erbium dopants or active pumping slowly spin down on their own

In figure 8, an optically trapped hexagon at a constant pressure with no atomic dopants gradually loses all its angular momentum to the surrounding gas molecules over a period of 0.5hrs, the rotational frequency spins down from 10KHz to about 5KHz before resuming a stable trapping configuration in the standing wave.

E. Particle Synthesis and Characterization

Undoped and 5% Er: β -NaYF disks were synthesized following the hydrothermal procedure developed by Felsted et al. with slight alterations [64]. Yttrium(III) ($YCl_3 \cdot 6 H_2O$, >99.999%, Sigma Aldrich) and for the doped case erbium(III) chloride hexahydrate ($ErCl_3 \cdot 6 H_2O$, >99.9%, Sigma Aldrich) were dissolved in ultrapure water (Barnstead GenPure) to ob-

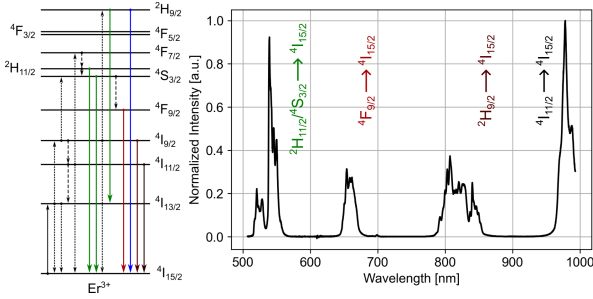


FIG. 10. Energy level diagram of erbium and measured up-conversion of Er:β-NaYF under 1560 nm illumination.

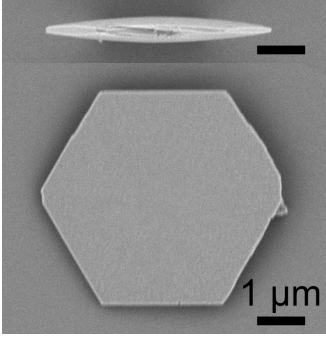


FIG. 11. SEM images of synthesized 5% erbium doped β-NaYF microcrystals. Note the slightly non regular geometry of the hexagon - this will lead to a slight mass asymmetry around all possible axes of rotation.

tain 4 mL of rare-earth solution containing a total of 1.125 mmol. Ethylenediaminetetraacetic acid (EDTA, >99.995%, Sigma Aldrich) was dissolved in H₂O using 5 M sodium hydroxide solution (obtained from >97% NaOH, Fisher Chemical) to nominally obtain 5 mL Na₂EDTA solution containing 1.125 mmol. The chelat-

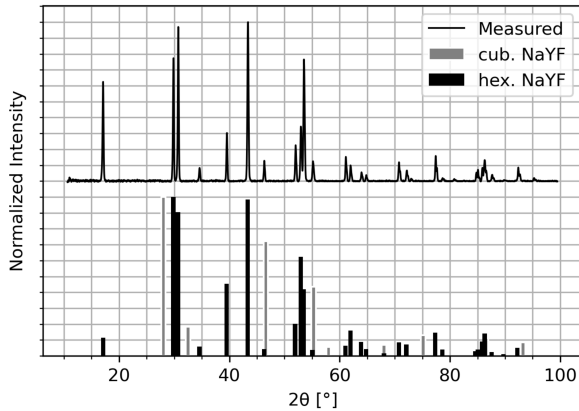


FIG. 12. XRD pattern of synthesized 5% erbium doped β-NaYF microcrystals. A comparison with database entries of cubic α-NaYF (PDF 01-075-6676) and hexagonal β-NaYF (01-092-0779) indicates phase purity.

ing solution was added to the rare-earth solution in a Teflon liner while stirring and stirred for 10 min. The fluoride precursor solution was obtained by dissolving 4.5 mmol (NaF, >99.5%, EMD Chemicals) in water to obtain 5 mL. After adding the fluoride solution to the chelated rare-earth solution under stirring and consecutive mixing for 30 min the Teflon liner was closed and placed in a hydrothermal autoclave (Parr Instruments 4747). The autoclave was transferred into a preheated oven (Thermo Scientific Heratherm) at 220 °C and the synthesis allowed to proceed for 72 h. The precipitate was collected by centrifugation after removing the autoclave from the hot oven and natural cooling to room temperature. The undoped or 5% Er:β-NaYF was washed three times each using 30 mL of H₂O or ethanol (200 proof, Decon Labs.) and dried in an oven at roughly 80 °C. To remove any remaining surface adsorbed EDTA the dry powder was calcined in a tube furnace (Thermo Scientific Lindberg/Blue M) at 300 °C with a 30 min ramp and 4 h hold.

Scanning electron microscopy images were obtained on an Apreo 2 (Thermo Fisher Scientific) using an acceleration voltage of 2 kV, a current of 13 pA and a backscatter detector.

Powder X-ray diffraction patterns are obtained using a Cu X-ray source operated at 50 kV and 1000 μA and a 2D detector (Pilatus 100K) on a Bruker D8 Discover.

Upconversion spectroscopy of the 5% Er:β-NaYF was obtained by illuminating dry powder on a cover slip using a tunable telecom laser (Santec TSL-710) focused by a 50x objective (Mitutoyo Plan Apo NIR). The spot sizes are around 5.5 μm resulting in irradiances from 1.0 kW/cm² to 1.1 kW/cm². The photoluminescence was collected by a second 50x objective (Mitutoyo Plan Apo NIR) and measured using an EM-CCD (BLAZE 100-HR, Princeton Instruments) mounted on a spectrometer (HRS-500, Princeton Instruments) after passing a 1000 nm short-pass filter (FESH1000, Thorlabs).

Material characterization results are presented in Figures 11 and 12. The mean particle diameter and height were (4.9 ± 1.0) μm and (210 ± 60) nm. The XRD pattern indicates phase pure β-NaYF.

ACKNOWLEDGEMENTS

AAG is supported in part by NSF grants PHY-2110524 and PHY-2111544, the Heising-Simons Foundation, the John Templeton Foundation. AAG and GW are supported by the W.M. Keck Foundation. AAG ZW and GW are supported by the DARPA levitas disruption engineering program. AAG, PJP, LF, ZF are supported by ONR Grant N00014-18-1-2370. GW is supported by a NASA NIAC phase 2 subaward from DRAPER labs. This work was supported in part by a grant from LeviNet. This work used the Quest high performance computing facility at Northwestern. We thank the Shariar group for a loan of a PPCL pure photonics laser and we thank Ju-

lian Gamboa for guidance on how to use it. We thank Professor Tracy Northrup of IQQI, Innsbruck, Austria,

EU and Levinet (UK) for supporting Miriam M Florez's research time with the group. We thank the Barnard and Majumdar groups for lending us a Santec TSL-710 laser.

-
- [1] K. Zeng, X. Xu, Y. Wu, X. Wu, and D. Xiao, Optically levitated micro gyroscopes with an mhz rotational vaterite rotor, *Microsystems & Nanoengineering* **10**, 78 (2024).
- [2] M. Rademacher, A. Pontin, J. Gosling, P. Barker, and M. Toroš, Roto-translational optomechanics, arXiv preprint arXiv:2507.20905 (2025).
- [3] Z. Xu and T. Li, Detecting casimir torque with an optically levitated nanorod, *Phys. Rev. A* **96**, 033843 (2017).
- [4] P. Ju, Y. Jin, K. Shen, Y. Duan, Z. Xu, X. Gao, X. Ni, and T. Li, Near-field ghz rotation and sensing with an optically levitated nanodumbbell, *Nano Letters* **23**, 10157 (2023).
- [5] B. A. Stickler, B. Papendell, S. Kuhn, B. Schriniski, J. Millen, M. Arndt, and K. Hornberger, Probing macroscopic quantum superpositions with nanorotors, *New Journal of Physics* **20**, 122001 (2018).
- [6] R. Reimann, M. Doderer, E. Hebestreit, R. Diehl, M. Frimmer, D. Windey, F. Tebbenjohanns, and L. Novotny, Ghz rotation of an optically trapped nanoparticle in vacuum, *Physical review letters* **121**, 033602 (2018).
- [7] J. Ahn, Z. Xu, J. Bang, Y.-H. Deng, T. M. Hoang, Q. Han, R.-M. Ma, and T. Li, Optically levitated nanodumbbell torsion balance and ghz nanomechanical rotor, *Phys. Rev. Lett.* **121**, 033603 (2018).
- [8] A. Tonomura, J. Endo, T. Matsuda, T. Kawasaki, and H. Ezawa, Demonstration of single-electron buildup of an interference pattern, *American Journal of Physics* **57**, 117 (1989).
- [9] R. Colella, A. W. Overhauser, and S. A. Werner, Observation of gravitationally induced quantum interference, *Phys. Rev. Lett.* **34**, 1472 (1975).
- [10] S. A. Werner, J. L. Staudenmann, and R. Colella, Effect of Earth's rotation on the quantum mechanical phase of the neutron, *Phys. Rev. Lett.* **42**, 1103 (1979).
- [11] H. Rauch and S. A. Werner, *Neutron Interferometry: Lessons in Experimental Quantum Mechanics* (Second Edition, Oxford University Press, 2015).
- [12] J. B. Fixler, G. T. Foster, J. M. McGuirk, and M. A. Kasevich, Atom interferometer measurement of the Newtonian constant of gravity, *Science* **315**, 74 (2007).
- [13] P. Asenbaum, C. Overstreet, T. Kovachy, D. D. Brown, J. M. Hogan, and M. A. Kasevich, Phase Shift in an Atom Interferometer due to Spacetime Curvature across its Wave Function, *Phys. Rev. Lett.* **118**, 183602 (2017), arXiv:1610.03832 [physics.atom-ph].
- [14] C. Overstreet, P. Asenbaum, J. Curti, M. Kim, and M. A. Kasevich, Observation of a gravitational Aharonov-Bohm effect, *Science* **375**, abl7152 (2021).
- [15] O. Amit, Y. Margalit, O. Dobkowski, Z. Zhou, Y. Japha, M. Zimmermann, M. A. Efremov, F. A. Narducci, E. M. Rasel, W. P. Schleich, and R. Folman, T^3 stern-gerlach matter-wave interferometer, *Phys. Rev. Lett.* **123**, 083601 (2019).
- [16] Y. Margalit, O. Dobkowski, Z. Zhou, O. Amit, Y. Japha, S. Moukouri, D. Rohrllich, A. Mazumdar, S. Bose, C. Henkel, and R. Folman, Realization of a complete stern-gerlach interferometer: Toward a test of quantum gravity, *Science Advances* **7**, eabg2879 (2021).
- [17] S. Eibenberger, S. Gerlich, M. Arndt, M. Mayor, and J. Tüxen, Matter-wave interference with particles selected from a molecular library with masses exceeding 10000 amu, *Phys. Chem. Chem. Phys.* **15**, 14696 (2013), arXiv:1310.8343 [quant-ph].
- [18] Y. Y. Fein, P. Geyer, P. Zwick, F. Kiałka, S. Pedalino, M. Mayor, S. Gerlich, and M. Arndt, Quantum superposition of molecules beyond 25 kDa, *Nature Phys.* **15**, 1242 (2019).
- [19] S. Pedalino, B. E. Ramírez-Galindo, R. Ferstl, K. Hornberger, M. Arndt, and S. Gerlich, Probing quantum mechanics using nanoparticle schrödinger cats (2025), arXiv:2507.21211 [quant-ph].
- [20] O. Romero-Isart, Quantum superposition of massive objects and collapse models, *Phys. Rev. A* **84**, 052121 (2011).
- [21] M. Schut, P. Andriolo, M. Toroš, S. Bose, and A. Mazumdar, Expression for the decoherence rate due to air-molecule scattering in spatial qubits, *Phys. Rev. A* **111**, 042211 (2025), arXiv:2410.20910 [quant-ph].
- [22] J. Bateman, S. Nimmrichter, K. Hornberger, and H. Ulbricht, Near-field interferometry of a free-falling nanoparticle from a point-like source, *Nature Communications* **5**, 4788 (2014).
- [23] A. Geraci and H. Goldman, Sensing short range forces with a nanosphere matter-wave interferometer, *Phys. Rev. D* **92**, 062002 (2015).
- [24] U. Delić, M. Reisenbauer, K. Dare, D. Grass, V. Vuletić, N. Kiesel, and M. Aspelmeyer, Cooling of a levitated nanoparticle to the motional quantum ground state, *Science* **367**, 892 (2020).
- [25] F. Tebbenjohanns, M. Frimmer, A. Militaru, V. Jain, and L. Novotny, Cold damping of an optically levitated nanoparticle to microkelvin temperatures, *Phys. Rev. Lett.* **122**, 223601 (2019).
- [26] M. Kamba, R. Shimizu, and K. Aikawa, Optical cold damping of neutral nanoparticles near the ground state in an optical lattice, *Opt. Express* **30**, 26716 (2022).
- [27] A. Ranfagni, K. Børkje, F. Marino, and F. Marin, Two-dimensional quantum motion of a levitated nanosphere, *Phys. Rev. Res.* **4**, 033051 (2022).
- [28] L. Dania, O. S. Kremer, J. Piotrowski, D. Candoli, J. Vijayan, O. Romero-Isart, C. Gonzalez-Ballester, L. Novotny, and M. Frimmer, High-purity quantum optomechanics at room temperature, *Nature Physics* **21**, 1603 (2025).
- [29] M. Rossi, A. Militaru, N. Carlon Zambon, A. Riera-Campenay, O. Romero-Isart, M. Frimmer, and L. Novotny, Quantum delocalization of a levitated nanoparticle, *Phys. Rev. Lett.* **135**, 083601 (2025).

- [30] S. Nimmrichter, *Macroscopic matter wave interferometry* (Springer, 2014).
- [31] L. Neumeier, M. A. Ciampini, O. Romero-Isart, M. Aspelmeyer, and N. Kiesel, Fast quantum interference of a nanoparticle via optical potential control, *Proceedings of the National Academy of Sciences* **121**, e2306953121 (2024).
- [32] Y. Ma, K. E. Khosla, B. A. Stickler, and M. Kim, Quantum persistent tennis racket dynamics of nanorotors, *Physical Review Letters* **125**, 053604 (2020).
- [33] J. Gao, F. van der Laan, J. A. Zielińska, A. Militaru, L. Novotny, and M. Frimmer, Feedback cooling a levitated nanoparticle's libration to below 100 phonons, *Physical Review Research* **6**, 033009 (2024).
- [34] T. Westphal, H. Hepach, J. Pfaff, and M. Aspelmeyer, Measurement of gravitational coupling between millimetre-sized masses, *Nature* **591**, 225 (2021).
- [35] S. M. Fleischer, M. P. Ross, K. Venkateswara, C. A. Hagedorn, E. A. Shaw, E. Swanson, B. Heckel, and J. Gundlach, A cryogenic torsion balance using a liquid-cryogen free, ultra-low vibration cryostat, *Review of Scientific Instruments* **93** (2022).
- [36] J. Ahn, Z. Xu, J. Bang, P. Ju, X. Gao, and T. Li, Ultrasensitive torque detection with an optically levitated nanorotor, *Nature nanotechnology* **15**, 89 (2020).
- [37] J. Zielińska, F. van der Laan, A. Norrman, R. Reimann, M. Frimmer, and L. Novotny, Long-axis spinning of an optically levitated particle: A levitated spinning top, *Physical Review Letters* **132**, 253601 (2024).
- [38] G. Winstone, Z. Wang, S. Klomp, G. R. Felsted, A. Laeuger, C. Gupta, D. Grass, N. Aggarwal, J. Sprague, P. J. Pauzauskie, et al., Optical trapping of high-aspect-ratio nanofabricated hexagonal prisms for kHz-mHz gravitational wave detectors, *Physical review letters* **129**, 053604 (2022).
- [39] N. Aggarwal, G. P. Winstone, M. Teo, M. Baryakhtar, S. L. Larson, V. Kalogera, and A. A. Geraci, Searching for new physics with a levitated-sensor-based gravitational-wave detector, *Physical Review Letters* **128**, 111101 (2022).
- [40] A. Rahman and P. Barker, A laser cooled nanocryostat: Refrigeration, alignment and rotation of levitated Yb^{3+} nanocrystals, arXiv preprint arXiv:1703.07155 (2017).
- [41] C. Laplane, P. Ren, R. P. Roberts, Y. Lu, and T. Volz, Inert shell coating for enhanced laser refrigeration of nanoparticles: application in levitated optomechanics, *ACS Photonics* **11**, 963 (2024).
- [42] S. Kuhn, A. Kosloff, B. A. Stickler, F. Patolsky, K. Hornberger, M. Arndt, and J. Millen, Full rotational control of levitated silicon nanorods, *Optica* **4**, 356 (2017).
- [43] Y. Arita, S. H. Simpson, G. D. Bruce, E. M. Wright, P. Zemánek, and K. Dholakia, Cooling the optical-spin driven limit cycle oscillations of a levitated gyroscope, *Communications Physics* **6**, 238 (2023).
- [44] Y. Hu, J. J. Kingsley-Smith, M. Nikkhou, J. A. Sabin, F. J. Rodríguez-Fortuño, X. Xu, and J. Millen, Structured transverse orbital angular momentum probed by a levitated optomechanical sensor, *Nature Communications* **14**, 2638 (2023).
- [45] M. Rashid, M. Toroš, A. Setter, and H. Ulbricht, Precision motion in levitated optomechanics, *Physical review letters* **121**, 253601 (2018).
- [46] J. Bang, T. Seberson, P. Ju, J. Ahn, Z. Xu, X. Gao, F. Robicheaux, and T. Li, Five-dimensional cooling and nonlinear dynamics of an optically levitated nanodumbbell, *Physical Review Research* **2**, 043054 (2020).
- [47] M. Kamba, R. Shimizu, and K. Aikawa, Nanoscale feedback control of six degrees of freedom of a near-sphere, *Nature Communications* **14**, 7943 (2023).
- [48] A. Pontin, H. Fu, M. Toroš, T. S. Monteiro, and P. F. Barker, Simultaneous cavity cooling of all six degrees of freedom of a levitated nanoparticle, *Nature Physics* **19**, 1003 (2023).
- [49] D. W. Keith, Photophoretic levitation of engineered aerosols for geoengineering, *Proceedings of the National Academy of Sciences* **107**, 16428 (2010).
- [50] J. Millen, T. Deesuwana, P. Barker, and J. Anders, Nanoscale temperature measurements using non-equilibrium brownian dynamics of a levitated nanosphere, *Nature nanotechnology* **9**, 425 (2014).
- [51] G. Ranjit, D. P. Atherton, J. H. Stutz, M. Cunningham, and A. A. Geraci, Attonewton force detection using microspheres in a dual-beam optical trap in high vacuum, *Physical Review A* **91**, 051805 (2015).
- [52] A. Cavalleri, G. Ciani, R. Dolesi, M. Hueller, D. Nicolodi, D. Tombolato, S. Vitale, P. Wass, and W. Weber, Gas damping force noise on a macroscopic test body in an infinite gas reservoir, *Physics Letters A* **374**, 3365 (2010).
- [53] A. Ivaturi, S. K. W. MacDougall, R. Martín-Rodríguez, M. Quintanilla, J. Marques-Hueso, K. W. Krämer, A. Meijerink, and B. S. Richards, Optimizing infrared to near infrared upconversion quantum yield of $\beta\text{-NaYF}_4\text{:Er}^{3+}$ in fluoropolymer matrix for photovoltaic devices, *Journal of Applied Physics* **114**, 013505 (2013).
- [54] S. Laing, S. Klomp, G. Winstone, A. Grinin, A. Dana, Z. Wang, K. S. Widyatmodjo, J. Bateman, and A. A. Geraci, Optimal displacement detection of arbitrarily-shaped levitated dielectric objects using optical radiation, arXiv preprint arXiv:2409.00782 (2024).
- [55] S. Kuhn, B. A. Stickler, A. Kosloff, F. Patolsky, K. Hornberger, M. Arndt, and J. Millen, Optically driven ultra-stable nanomechanical rotor, *Nature communications* **8**, 1670 (2017).
- [56] L. Van Damme, P. Mardešić, and D. Sugny, The tennis racket effect in a three-dimensional rigid body, *Physica D: Nonlinear Phenomena* **338**, 17 (2017).
- [57] NASA, Dzhanibekov effect (video), https://en.wikipedia.org/wiki/File:Dzhanibekov_effect.ogg (2015), public domain (US government work).
- [58] C. Rennero-Lecuna, R. Martín-Rodríguez, R. Valiente, J. González, F. Rodríguez, K. W. Krämer, and H. U. Güdel, Origin of the High Upconversion Green Luminescence Efficiency in $\beta\text{-NaYF}_4\text{:2\%Er}^{3+},\text{20\%Yb}^{3+}$, *Chemistry of Materials* **23**, 3442 (2011).
- [59] X. Xia, A. Volpi, J. Y. D. Roh, M. C. De Siena, D. R. Gamelin, M. P. Hehlen, and P. J. Pauzauskie, The impact of $2\text{H} \rightarrow 4\text{I}$ emission from Er^{3+} ions on ratiometric optical temperature sensing with $\text{Yb}^{3+}/\text{Er}^{3+}$ co-doped upconversion materials, *Journal of Luminescence* **236**, 118006 (2021).
- [60] E. Ortiz-Rivero, K. Prorok, I. R. Martín, R. Lisiecki, P. Haro-González, A. Bednarkiewicz, and D. Jaque, Laser refrigeration by an ytterbium-doped nanofabricated microspinning, *Small* **17**, 2103122 (2021).
- [61] C. R. Harris, K. J. Millman, S. J. van der Walt, et al., Array programming with numpy, *Nature* **585**, 357 (2020).

- [62] P. Virtanen, R. Gommers, T. E. Oliphant, M. Haberland, T. Reddy, D. Cournapeau, E. Burovski, P. Peterson, W. Weckesser, J. Bright, S. J. van der Walt, M. Brett, J. Wilson, K. J. Millman, N. Mayorov, A. R. J. Nelson, E. Jones, R. Kern, E. Larson, C. Carey, Í. Polat, Y. Feng, E. W. Moore, J. VanderPlas, D. Laxalde, J. Perktold, R. Cimrman, I. Henriksen, E. A. Quintero, C. R. Harris, A. M. Archibald, A. H. Ribeiro, F. Pedregosa, P. van Mulbregt, and SciPy 1.0 Contributors, SciPy 1.0: Fundamental algorithms for scientific computing in python, *Nature Methods* **17**, 261 (2020).
- [63] J. D. Hunter, Matplotlib: A 2d graphics environment, *Computing in Science & Engineering* **9**, 90 (2007).
- [64] R. Felsted, A. Pant, A. Bard, X. Xia, D. Luntz-Martin, S. Dadras, Siamak; zhang, A. Vamivakas, and P. Pauzauskie, Chemically tunable aspect ratio control and laser refrigeration of hexagonal sodium yttrium fluoride upconverting materials, *Crystal Growth and Design* (2022).